JOURNAL OF COMPUTATIONAL PHYSICS 106, 355–365 (1993)

A Fast Algorithm to Solve the Beltrami Equation with Applications to Quasiconformal Mappings

PRABIR DARIPA

Department of Mathematics, Texas A & M University, College Station, Texas 77843

Received August 16, 1991

Two algorithms are provided for the fast and accurate computation of the solution of Beltrami equations in the complex plane in the interior of a unit disk. There are two integral operators which are fundamental in the construction of this solution. A fast algorithm to evaluate one of these integrals is given by Daripa (*SIAM J. Sci. Stat. Comput.*, Nov. 1992). An algorithm for fast evaluation of the second integral is provided here. These algorithms are based on representation of the solution in terms of a double integral, some recursive relations in Fourier space, and fast Fourier transforms. The theoretical computational complexity of our algorithm is $O(MN \ln N)$, where M and N are the number of nodes in the circular and radial directions. We show the application of these algorithms in constructing numerical methods for quasiconformal mappings. A numerical method is provided and explored numerically for the construction of quasiconformal mappings using the Beltrami equation. In particular we show the effect of dilatations on the Jacobian of the mappings which controls what is known as the crowding phenomenon in the literature.

1. INTRODUCTION

Beltrami equations arise in many areas of pure and applied mathematics such as quasiconformal mappings [1, 10, 11], fluid mechanics [6], electrostatics [10], and more generally in the transformation of a quasilinear partial differential equation to canonical form [4]. These equations are given by

$$u_{\bar\sigma} = \mu(\sigma)\, u_\sigma, \tag{1}$$

where μ and u are complex valued functions of complex variables σ and $\bar\sigma$. Henceforth a subscript denotes derivative with respect to that variable and an overbar denotes complex conjugation. Here and below the generalized derivatives ∂_σ and $\partial_{\bar\sigma}$ denote respectively

$$\partial_\sigma = \tfrac{1}{2}(\partial_x - i\partial_y), \qquad \partial_{\bar\sigma} = \tfrac{1}{2}(\partial_x + i\partial_y), \tag{2}$$

and

$$\sigma = x + iy. \tag{3}$$

In this paper we are interested in constructing a fast and accurate algorithm to solve Eq. (1) in the unit disk $|\sigma| \leqslant 1$ and its application to quasiconformal mapping.

Quasiconformal mappings (occasionally we refer to these as Q-mappings) are a generalization of conformal mappings [1, 10, 11]. Quasiconformal mappings, $w = f(\sigma)$, map a region Ω_σ in the σ-plane to a region Ω_w in the w-plane. Such a mapping is conformal in an appropriate Riemannian metric and it preserves angles almost everywhere if these are measured in the region Ω_σ in terms of the Riemann metric but in the region Ω_w in terms of usual Euclidean metric. At a point σ_0, such a mapping induces a linear mapping and maps circles into ellipses. The orientation and aspect ratio of the ellipses characterize these mappings. There are some striking relations between these characteristics and the generalized derivatives of the mapping function [1, 10, 11]. These relations allow the reformulation of the quasiconformal mapping as a homeomorphic generalized solution $w = f(\sigma)$ of Beltrami's equation: $w_{\bar\sigma} - \mu(\sigma)\, w_\sigma = 0$, where $\mu(\sigma)$, called a complex dilatation, is a measurable function in Ω_σ that satisfies some appropriate conditions. This complex dilatation is related to the characteristics of the mapping referred to earlier. Thus, generating quasiconformal mappings with any desired characteristics amounts to solving the Beltrami equation with pre-assigned values of the complex dilatation in Ω_σ.

There are many advantages to constructing these mappings as mentioned in Ahlfors [1]. Many problems in applied fields can be viewed as problems in Q-mappings. Our interest in this paper, however, is from the viewpoint of flexibility that it provides over conformal mappings. Conformal mapping is known to suffer from two serious deficiencies. One is a direct by-product of Riemann's mapping theorem: it does not provide very many flexible parameters to be adjusted. Therefore, within this framework, there is no cure for the crowding phenomenon unless the domain itself is changed. This problem of the crowding phenomenon can possibly be handled very effectively by Q-mapping. Second is the problem with the convergence of

0021-9991/93 $5.00

numerical conformal mapping methods. In quasiconformal mapping, an appropriate choice of dilatation may help in this regard. Thus Q-mappings are less rigid than conformal mappings and therefore can be very effective as a tool.

There are various general methods for conformal mapping of an arbitrary domain into a circular domain, e.g., Theodorsen's, Timman's, Freiberg's, Wegmann's, etc. [9]. Not all of these methods succeed in all problems and the methods which succeed in a particular problem have their own special characteristics from the viewpoint of convergence and accuracy. Some of these methods when used in connection with time dependent problems may succeed at earlier times but fail at later times due to the crowding phenomenon. Quasiconformal mappings may provide a viable way to adjust the resolution by an appropriate choice of time dependent dilation so that time dependent nonlinear physical problems can be probed numerically far into the nonlinear regime. This also calls for developing as many numerical methods as possible for generating quasiconformal mappings. To the best of the author's knowledge, there is no constructive numerical method for quasiconformal mappings using the Beltrami equation (1). In Section 3, we describe a numerical method for numerical construction of quasiconformal mappings.

The rest of the paper is laid out as follows. In Section 2, we discuss the Beltrami equation and a fast method for accurate evaluation of certain integral operators arising in the context of Beltrami equation. Section 3 discusses a numerical method for quasiconformal mappings using the Beltrami equation (1). We carry out some numerical experiments with this method in Section 3. Conclusions are presented in Section 4. In a subsequent article, we will generalize various conformal mapping methods to the quasiconformal case.

2. BELTRAMI EQUATION

2.1. *Preliminaries*

In this section we briefly describe some of the relevant facts about the Beltrami equation which are needed for solving this equation with appropriate boundary data. We consider the Beltrami equation:

$$u_{\bar\sigma} = \mu(\sigma)\, u_\sigma \equiv h(\sigma) \tag{4}$$

in Ω_σ: $|\sigma| \leqslant 1$, where $|\mu(\sigma)| \leqslant K < 1$ and is Hölder continuous with exponent α. The solution to this equation is usually written in terms of the following two integral operators:

$$Ph(\sigma) = -\frac{1}{\pi}\iint_{\Omega_\sigma} \frac{h(\sigma)}{\zeta - \sigma}\, d\xi\, d\eta \tag{5}$$

and

$$Th(\sigma) = -\frac{1}{\pi}\iint_{\Omega_\sigma} \frac{h(\sigma)}{(\zeta - \sigma)^2}\, d\xi\, d\eta, \tag{6}$$

where $\zeta = \xi + i\eta$. The operator T is to be understood as a Cauchy principal value and the function $h(\sigma)$ will be assumed to be in C_0^2, decaying at least quadratically as $\sigma \to 0$ [1]. These two integral operators, $Ph(\cdot)$ and $Th(\cdot)$, will often be termed as P-transform and T-transform, respectively. These two integral operators are known to satisfy the following relations:

$$(Ph)_{\bar\sigma} = h, \tag{7}$$

$$(Ph)_\sigma = Th. \tag{8}$$

The solution of Eq. (4) can be written as

$$u(\sigma) = Ph(\sigma) + g(\sigma), \tag{9}$$

where $g(\sigma)$ is a suitable analytic function. The precise form of this function depends on the boundary data. For later reference, we should note the following relation which follows from (4), (8), and (9):

$$h(\sigma) = \mu(\sigma)(Th(\sigma) + g_\sigma(\sigma)). \tag{10}$$

In the following section we describe some fast algorithms to solve the boundary value problem associated with (4). This will be the building block for the construction of quasiconformal mappings which we describe in Section 3.

2.2. *Dirichlet Problem and Its Solution Algorithm*

We are interested in solving the following problem: find a $u(\sigma)$ in $|\sigma| \leqslant 1$ such that

$$\begin{aligned} &u_{\bar\sigma} = \mu(\sigma)\, u_\sigma \equiv h(\sigma); && |\sigma| \leqslant 1, \\ &\text{Real}[u(\sigma = e^{i\alpha})] = u_0(\alpha); && 0 \leqslant \alpha \leqslant 2\pi, \\ &\text{Imag}[u(\sigma = 0)] = v_0. \end{aligned} \tag{P}$$

The function $\mu(\sigma)$ will be assumed to be in C_0^2 (i.e., C^2 with compact support near the origin). It is known that this problem has a unique solution [1, 4].

Since $h(\sigma)$ $(= \mu(\sigma)\, u_\sigma)$ itself depends on $u(\sigma)$, an iterative algorithm has to be used to construct a solution of the problem (P). However, at each iteration level, the solution procedure is based on representation of $u(\sigma)$ as a P-transform of $h(\sigma)$ except for an additive analytic function $g(\sigma)$ (see (6)). It then follows from (9) and problem (P) that at each iteration level, the function $g(\sigma)$ is to be updated as a

solution of the following problem: find a $g(\sigma)$ in $|\sigma| \leqslant 1$ such that

$$\begin{aligned} g_{\bar{\sigma}} &= 0; \qquad |\sigma| \leqslant 1, \\ \text{Real}[g(\sigma = e^{i\alpha})] &= u_0(\alpha) - \text{Real}(Ph(\sigma = e^{i\alpha})); \\ & \qquad 0 \leqslant \alpha \leqslant 2\pi, \\ \text{Imag}[g(\sigma = 0)] &= v_0 - \text{Imag}(Ph(\sigma = 0)). \end{aligned} \tag{RP}$$

This is a standard problem in the theory of complex variables and the solution to this problem can easily be constructed [7]. We denote the solution by

$$g(\sigma) = \Lambda(Ph^k(\alpha); u_0(\alpha), v_0), \tag{11}$$

where Λ denotes the solution operator of the above problem. Once this problem has been solved, the solution of problem (P) is constructed from (9), assuming that $h(\sigma)$ and $Ph(\sigma)$ are known in $|\sigma| \leqslant 1$. We describe the following two algorithms based on how one calculates $h(\sigma)$.

ALGORITHM I. We see the Eq. (4), (9), and (11) suggest the following iteration scheme:

$$g^k(\sigma) = \Lambda(Ph^k(\alpha); u_0(\alpha), v_0) \tag{12}$$

$$u^k(\sigma) = Ph^k(\sigma) + g^k(\sigma) \tag{13}$$

$$h^{k+1}(\sigma) = \mu(\sigma)(u^k(\sigma))_\sigma. \tag{14}$$

Here the superscript "k" refers to the level of iteration. It is obvious that a suitable initial choice of $h^k(\sigma)$ starts the iteration procedure. Thereafter each level of iteration involves the following four steps:

(1) Find the P-transform $Ph(\sigma)$ using the algorithm described in [7] *in the entire domain.* As shown in [7], the algorithmic complexity of this stage of the computation is at worst $MN \ln N$ with MN grid points in the discretization of the unit disk (the grid-system in the unit disk consists of N radial and M circular lines).

(2) Construct the analytic function $g(\sigma)$ in $|\sigma| \leqslant 1$ by solving the reduced problem (RP). This also involves an algorithmic complexity of the order $O(MN \ln N)$ [7].

(3) Construct the solution $u^k(\sigma)$ by adding the above two solutions according to (9).

(4) Evaluate the derivative $u^k_\sigma(\sigma)$ from known values of $u^k(\sigma)$ using the definition in (2).

In the fourth step of Algorithm I, the *accurate* evaluation of $u^k_\sigma(\sigma)$ from known values of $u^k(\sigma)$ at discrete polar lattice points (the grid-system in the unit disk consists of radial and circular lines) is a difficult task. Since the operator ∂_σ is defined in terms of Cartesian co-ordinates (see (2)) and the numerical values of $u(\sigma)$ are known on the polar grid points, the evaluation of $u^k_\sigma(\sigma)$ at the grid points requires some sort of approximation. We mention two types of approximation which seem reasonable. One way to evaluate this would be to take the mean of two directional derivatives, with the local directions being the radial and its orthogonal. Another way would be to first project locally the known values of $u^k(\sigma)$ from the polar system to the Cartesian system and then use these values to evaluate the derivative using equation (2).

We mention the following algorithm which avoids direct evaluation of these derivatives completely and is better than the first algorithm from the viewpoint of accuracy. This also has the same algorithmic complexity as Algorithm I.

ALGORITHM II. We see that Eqs. (10) and (11) suggest the following iteration scheme:

$$g^k(\sigma) = \Lambda(Ph^k(\alpha); u_0(\alpha), v_0) \tag{15}$$

$$h^{k+1}(\sigma) = \mu(\sigma)[Th^k(\sigma) + g^k_\sigma(\sigma)]. \tag{16}$$

Similar to Algorithm I, here also a suitable initial choice of $h^k(\sigma)$ starts the iteration procedure. Thereafter each level of iteration involves the following three steps:

(1) Find the P-transform $Ph(\alpha)$ using the algorithm described in [7] *only on the unit circle.* As shown in [7], the algorithmic complexity of this stage of the computation is at worst $MN \ln N$ with MN grid points in the discretization of the unit disk.

(2) Construct the analytic function $g(\sigma)$ by solving the reduced problem (RP).

(3) Find the T-transform $Th(\sigma)$ in the entire domain using the algorithm described in Section 2.4.

(4) Update $h(\sigma)$ using Eq. (16).

We should mention here that both the algorithms have the same operation count, provided the T-transform is calculated by a fast transform described in Section 2.4. Daripa [7] provides a fast algorithm to evaluate $Ph(\sigma)$. Ideas similar to that in [7] are used to derive the fast algorithm to evaluate $Th(\sigma)$ which we describe below.

Remarks 2.1. Note that the above two algorithms update $h(\sigma)$ at the end of each iteration and this updated $h(\sigma)$ becomes the input for the next iteration. The rate of convergence of the above scheme to the exact solution will depend crucially on the initial guess of $h(\sigma)$. The fact that $h(\sigma) = \mu(\sigma)\, u_\sigma$ suggests an initial guess of $h(\sigma) = 0$ if $\mu(\sigma)$ is chosen to be $O(\varepsilon)$ in the unit disk where ε is small.

2.3. Evaluation of *P*-transform

A fast algorithm to evaluate this transform has been given by Daripa [7].

2.4. Evaluation of *T*-transform

The evaluation of the T-transform can be performed by an algorithm which is similar to that in Daripa [7]. We give a detailed derivation of this algorithm below since there are some subtle differences in various stages due to the principal value nature of this transform.

2.4.1. *Mathematical Foundation of the Algorithm*

In this section we develop the theory needed to construct an efficient algorithm for the evaluation of the T-transform. In the following we use the notations Ω_r: $|\sigma| \leqslant r < 1$, $\Omega_{\bar{r}}$: $\Omega \backslash \Omega_r$, and Ω_{ij}: $r_i \leqslant |\sigma| \leqslant r_j$. The following theorem is crucial for the later development of the algorithm.

THEOREM 2.1. *The T-transform of* $h(\sigma)$ *with* $\sigma = re^{i\alpha}$ *can be written as*

$$Th(\sigma) = \sum_{n=-\infty}^{\infty} c_n(r)\, e^{in\alpha}, \tag{17}$$

where

$$c_n(r) = \begin{cases} \dfrac{n+1}{r\pi} \iint_{\Omega_r} h(\zeta) \left(\dfrac{r}{\zeta}\right)^{n+1} \left(\dfrac{1}{\zeta}\right) d\xi\, d\eta; & n < 0, \\ -\dfrac{n+1}{r\pi} \iint_{\Omega_{\bar{r}}} h(\zeta) \left(\dfrac{r}{\zeta}\right)^{n+1} \left(\dfrac{1}{\zeta}\right) d\xi\, d\eta; & n \geqslant 0. \end{cases} \tag{18}$$

Proof. We expand the T-transform defined in (6) in a Fourier series, i.e.,

$$-\frac{1}{\pi} \iint_{\Omega} \frac{h(\zeta)}{(\zeta - re^{i\alpha})^2}\, d\xi\, d\eta = \sum_{n=-\infty}^{\infty} c_n(r)\, e^{in\alpha}. \tag{19}$$

It follows that

$$\begin{aligned} -\pi c_n(r) &= \frac{1}{2\pi} \int_0^{2\pi} e^{-in\alpha} \left(\iint_{\Omega} \frac{h(\zeta)}{(\zeta - re^{i\alpha})^2}\, d\xi\, d\eta \right) d\alpha \\ &= \frac{1}{2\pi} \iint_{\Omega} h(\zeta)\, Q_n(r, \zeta)\, d\xi\, d\eta, \end{aligned} \tag{20}$$

where

$$Q_n(r, \zeta) = \int_0^{2\pi} \frac{e^{-in\alpha}}{(\zeta - re^{i\alpha})^2}\, d\alpha. \tag{21}$$

It is an elementary exercise in complex variable theory to show that

$$Q_n(r, \zeta) = -2\pi r^n T_n(\zeta), \tag{22}$$

where

$$T_n(\zeta) = -\delta(n)(n+1)\, \zeta^{-(n+2)} + \begin{cases} (n+1)\, \zeta^{-(n+2)}; & |\zeta| < |\sigma|, \\ 0.5(n+1)\, \zeta^{-(n+2)}; & |\zeta| = |\sigma|, \\ 0; & |\zeta| > |\sigma|. \end{cases} \tag{23}$$

In (23), $\delta(n) = 0$ for $n < 0$ and $\delta(n) = 1$ for $n \geqslant 0$. Substitution of (22) in (20) gives

$$c_n(r) = \frac{r^n}{\pi} \iint_{\Omega} h(\zeta)\, T_n(\zeta)\, d\xi\, d\eta. \tag{24}$$

Substitution of (23) in (24) yields the desired result, i.e., (18).

Remark 2.2. The above theorem can also be derived by first expanding $1/(\zeta - \sigma)$ in powers of ζ/σ and σ/ζ, followed by integration in the complex plane.

COROLLARY 2.1. *Suppose that* $\zeta = \rho e^{i\theta}$ *and*

$$h(\zeta) = \sum_{n=-\infty}^{\infty} h_n(\rho)\, e^{in\theta}. \tag{25}$$

Then the coefficients $c_n(r)$ *in* (18) *can be written as*

$$c_n(r) = \begin{cases} 2\dfrac{(n+1)}{r} \displaystyle\int_0^r h_{n+2}(\rho) \left(\frac{r}{\rho}\right)^{n+1} d\rho; & n < 0, \\ -2\dfrac{(n+1)}{r} \displaystyle\int_r^1 h_{n+2}(\rho) \left(\frac{r}{\rho}\right)^{n+1} d\rho; & n \geqslant 0. \end{cases} \tag{26}$$

Proof. Note first that $d\xi\, d\eta = \rho\, d\rho\, d\theta$ and $\zeta = \rho e^{i\theta}$. Substituting these in (18), we obtain

$$c_n(r) = \begin{cases} -\dfrac{n+1}{r\pi} \displaystyle\iint_{\Omega_r} h(\zeta) \left(\frac{r}{\rho}\right)^{n+1} e^{-i(n+2)\theta}\, d\theta\, d\rho; & n < 0, \\ -\dfrac{n+1}{r\pi} \displaystyle\iint_{\Omega_{\bar{r}}} h(\zeta) \left(\frac{r}{\rho}\right)^{n+1} e^{-i(n+2)\theta}\, d\theta\, d\rho; & n \geqslant 0. \end{cases} \tag{27}$$

Assertion (26) now follows from (25) and (27).

COROLLARY 2.2. *It follows directly from* (26) *that* $c_n(1) = 0$ *for* $n \geqslant 0$, $c_n(0) = 0$ $\forall n \neq 0$. *Similarly, it follows directly from* (25) *that* $h_n(0) = 0$ *for* $n \neq 0$, *and* $h_0(0) = h(0)$.

COROLLARY 2.3. *Let $r_j > r_i$. Define*

$$c_n^{ij} = 2\left(\frac{n+1}{R}\right)\int_{r_i}^{r_j} h_{n+2}(\rho)\left(\frac{R}{\rho}\right)^{n+1} d\rho, \tag{28}$$

where

$$R = \begin{cases} r_i; & n \geq 0, \\ r_j; & n < 0. \end{cases} \tag{29}$$

Then

$$c_n(r_j) = \left(\frac{r_j}{r_i}\right)^n c_n(r_i) + c_n^{ji}; \qquad n < 0, \tag{30}$$

and

$$c_n(r_i) = \left(\frac{r^i}{r_j}\right)^n c_n(r_j) - c_n^{ij}; \qquad n \geq 0. \tag{31}$$

Proof. For $n < 0$, we have from (26),

$$\begin{aligned} c_n(r_j) &= 2\left(\frac{n+1}{r_j}\right)\int_0^{r_j} h_{n+2}(\rho)\left(\frac{r_j}{\rho}\right)^{n+1} d\rho \\ &= 2\left(\frac{n+1}{r_j}\right)\int_0^{r_i} h_{n+2}(\rho)\left(\frac{r_i}{\rho}\right)^{n+1}\left(\frac{r_j}{r_i}\right)^{n+1} d\rho \\ &\quad + 2\left(\frac{n+1}{r_j}\right)\int_{r_i}^{r_j} h_{n+2}(\rho)\left(\frac{r_j}{\rho}\right)^{n+1} d\rho \\ &= \left(\frac{r_j}{r_i}\right)^n c_n(r_i) + c_n^{ij}. \end{aligned} \tag{32}$$

For $n \geq 0$, we have from (26),

$$\begin{aligned} c_n(r_i) &= -2\left(\frac{n+1}{r_j}\right)\int_{r_i}^{1} h_{n+2}(\rho)\left(\frac{r_i}{\rho}\right)^{n+1} d\rho \\ &= -2\left(\frac{n+1}{r_j}\right)\int_{r_i}^{r_j} h_{n+2}(\rho)\left(\frac{r_i}{\rho}\right)^{n+1} d\rho \\ &\quad - 2\left(\frac{n+1}{r_j}\right)\int_{r_j}^{1} h_{n+2}(\rho)\left(\frac{r_i}{\rho}\right)^{n+1} d\rho \\ &= \left(\frac{r_i}{r_j}\right)^n c_n(r_j) - c_n^{ij}. \end{aligned} \tag{33}$$

COROLLARY. *Let* $0 = r_1 < r_2 < r_3 \cdots < r_M = 1$. *Then* $c_n(r_l)$ *can be written as*

$$c_n(r_l) = \begin{cases} \displaystyle\sum_{i=2}^{l}\left(\frac{r_l}{r_i}\right)^n c_n^{i-1,i} \\ \quad \textit{for} \quad n < 0 \textit{ and } l = 2, \ldots, M, \\ \displaystyle -\sum_{i=l}^{M-1}\left(\frac{r_l}{r_i}\right)^n c_n^{i,i+1} \\ \quad \textit{for} \quad n \geq 0 \textit{ and } l = 1, \ldots, M-1. \end{cases} \tag{34}$$

Proof. Identical to that in [7] without any modification whatsoever.

2.4.2. *The Fast Algorithm*

We construct the fast algorithm based on the theory of Section 2. The unit disk is discretized using $M \times N$ lattice points with M equidistant points in the radial direction and N equidistant points in the circular direction.

Initialization

Choose M and N. Define $K = N/2$.

Step 1

For $l \in [1, M]$ and $n \in [-K+1, K]$, compute the Fourier coefficients $h_n(r_l)$ of $h(\zeta)$ from the known values of $h(\zeta = r_j e^{2\pi ik/N})$, $j = 1, \ldots, M$; $k = 1, \ldots, N$.

Step 2

Compute $c_n^{i,i+1}$, $i \in [1, M-1]$ for $n \in [-K-1, K-2]$, using (28).

Step 3

Compute the Fourier coefficients $c_n(r_l)$; $n \in [-K-1, K-2]$, $l \in [1, M]$, using the relations (30) and (31).

set $c_n(r_M) = 0\ \forall n \in [0, K-2]$
do $n = 0, \ldots, K-2$
  do $l = M-1, \ldots, 1$
  Use (31) of Corollary 2.4 to compute $c_n(r_l)$
  $c_n(r_l) = ((r_l/r_{l+1}))\, c_n(r_{l+1}) - c_n^{l,l+1}$
  enddo
enddo

set $c_n(r_1) = 0\ \forall n \in [-K-1, -1]$
do $n = -K-1, \ldots, -1$
  do $l = 2, \ldots, M$
  Use (30) of Corollary 2.4 to compute $c_n(r_l)$
  $c_n(r_l) = ((r_l/r_{l-1}))^n\, c_n(r_{l-1}) + c_n^{l-1,l}$
  enddo
enddo

Step 4

Finally compute $Th(\sigma = r_j e^{2\pi ik/N})$; $j \in [1, M]$, $k \in [1, N]$, using a truncated version of (17).

2.4.3. *The Algorithmic Complexity*

Here we consider the computational complexity of the above algorithm. We discuss the asymptotic operation count, the asymptotic time complexity and asymptotic storage requirement in order. A brief analysis of the algorithmic complexity follows:

Step	Operation count	Explanation
1	$O(MN \ln N)$	Each set of discrete Fourier transforms of N data sets contribute $N \ln N$ operations There are M such discrete Fourier transforms
2	$O(MN)$	For each n, computations of $c_n^{i,i+1}$, $i \in [1, M-1]$ contribute $2M$ operations There are N such computations for $n \in [-K-1, K-2]$
3	$O(MN)$	Computation of each $c_n(r_l)$ takes one operation There are $2MN$ such computations
4	$O(MN \ln N)$	Computation of $Ph(\sigma = r_j e^{i\alpha_k})$, $k \in [1, N]$ for each fixed "j" by FFT contributes $N \ln N$ operations There are M such FFTs to be performed.

From the above table we see that the asymptotic operation count and hence the asymptotic time complexity is $O(MN \ln N)$.

The algorithm requires storage of the MN Fourier coefficients $h_n(r_l)$ in Step 1, the MN Fourier coefficients $c_n(r_l)$ in Step 3 and the MN values of the desired Ph at MN grid points in Step 4. Therefore the asymptotic storage requirement is $O(MN)$.

Remark 2.3. The computation c_n^{ij} in Step 2 can be embedded within the inner do-loops of Step 3, thus avoiding the storage requirement for these. Note that we present the algorithm in the form as shown above for the sake of clarity and without any sacrifice in the asymptotic time complexity.

3. APPLICATIONS TO QUASICONFORMAL MAPPING

3.1. A Numerical Method

We seek a quasiconformal mapping of the interior of the unit disk $|\sigma| \leqslant 1$, onto the exterior of a simple, closed and smooth curve Γ in the z-plane such that the unit disk maps onto the curve Γ and the origin $\sigma = 0$ on to $z = \infty$. Coordinates in the z-plane are chosen so that $z = 0$ is inside the curve Γ. The curve Γ is such that it can be parametrized by ϕ as follows:

$$z(\phi) = \rho(\phi)\, e^{i\phi}, \qquad 0 \leqslant \phi \leqslant 2\pi. \tag{35}$$

We seek to construct the solution of this quasiconformal mapping problem which can be formulated as follows: find a $z(\sigma)$, $|\sigma| \leqslant 1$, such that

$$\begin{aligned} &z_{\bar{\sigma}} = \lambda(\sigma)\, z_\sigma; \qquad |\sigma| \leqslant 1, \\ &z(\sigma): \Gamma \to |\sigma| = 1, \\ &\lim_{\sigma \to 0} |z(\sigma)| = \infty. \end{aligned} \tag{QP}$$

Since the solution variable $z(\sigma)$ is singular at $\sigma = 0$, it will be convenient to reformulate the above problem into the following equivalent problem: find a $z(\sigma)$, $|\sigma| \leqslant 1$, such that

$$\begin{aligned} &w_{\bar{\sigma}} = \lambda(\sigma)(\ln z)_\sigma \equiv h(\sigma); \qquad |\sigma| \leqslant 1, \\ &z(\sigma): \Gamma \to |\sigma| = 1, \\ &|w(\sigma = 0)| = 0, \end{aligned} \tag{DQP}$$

where

$$w(\sigma) = \ln(z\sigma). \tag{36}$$

The complex dilatation $\lambda(\sigma)$ should be prescribed carefully as described in the next section. The formal statement of boundary correspondence in (DQP) can be translated into an appropriate equation which will be required in the solution algorithm for this problem. We have from (35) and (36),

$$\tilde{w}(\alpha) = \ln \tilde{\rho}(\alpha) + i(\phi + \alpha); \qquad 0 \leqslant \alpha \leqslant 2\pi, \tag{37}$$

where we have used

$$\tilde{w}(\alpha) = w(\sigma = e^{i\alpha}); \qquad \tilde{\rho}(\alpha) = \rho(\phi(\alpha)). \tag{38}$$

Note that the quasiconformal mapping problem (DQP) is now exactly identical to the problem (P) discussed in Section 2.2 except that the statement of boundary correspondence in (DQP) should be replaced by the following equation which follows from (37):

$$\text{Real}[\tilde{w}(\alpha)] = \ln \tilde{\rho}(\alpha). \tag{39}$$

Note that even though the $\tilde{\rho}(\alpha)$ is not known a priori, this can be updated during the iterative procedures of the solution algorithms mentioned in (2.2). Since $\rho(\phi)$ is known from (35), the $\tilde{\rho}(\alpha)$ can be updated from the equation

$$(\ln \tilde{\rho}(\alpha))^{k+1} = \ln \rho(\phi^k(\alpha)), \tag{40}$$

where

$$\phi^k(\alpha) = \text{Imag}[w^k(\alpha)] - \alpha, \tag{41}$$

which follows from (37). Here the superscripts k and $k+1$ refer to the level of iteration in the algorithms mentioned in Section 2.2.

3.2. Choice of Complex Dilatation $\lambda(\sigma)$

The Jacobian of the Q-mapping is given by [1]

$$J = |z_\sigma|^2 - |z_{\bar\sigma}|^2 = (1 - |\lambda(\sigma)|^2)\,|z_\sigma|^2. \tag{42}$$

Note that the mapping is sense preserving if

$$|\lambda(\sigma)| < 1, \qquad \text{in} \quad |\sigma| \leqslant 1. \tag{43}$$

Also $\lambda(\sigma)$ should be chosen so that $\lambda(\sigma) \sim O(\sigma^3)$ as $\sigma \to 0$. This and Eq. (43) will guarantee that the solution to the quasiconformal mapping problem exists for the following reasons. From (DQP) we can write

$$w(\sigma) = Ph(\sigma) + g(\sigma) \tag{44}$$

and

$$w_\sigma(\sigma) = Th(\sigma) + g_\sigma(\sigma), \tag{45}$$

where $g(\sigma)$ is an analytic function. We assume a priori that $h(\sigma)$ is in C_0^2 and therefore the T-transform is well defined and is in C^1 [1]. Therefore it follows from (45) that

$$w_\sigma(\sigma) \sim O(1) \qquad \text{as} \quad \sigma \to 0; \tag{46}$$

whence from using (36), we have

$$(\ln z)_\sigma \sim O\left(\frac{1}{\sigma}\right) \qquad \text{as} \quad \sigma \to 0. \tag{47}$$

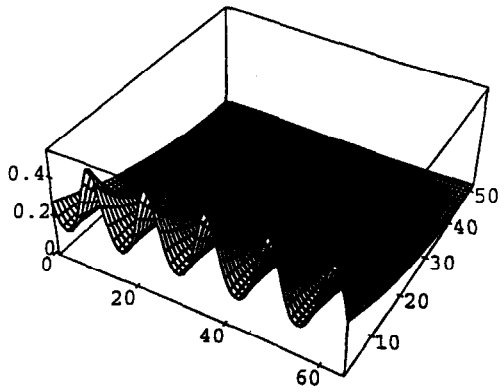

FIG. 1. Absolute value of the complex dilatation, $\lambda = |\sigma|^2\, e^{0.65(i\sigma^5 - 2.0)}$, where $\sigma = re^{i\alpha}$; $0 \leqslant r \leqslant 1$, $0 \leqslant \alpha \leqslant 2\pi$. The plot is shown here in rectangular co-ordinate system where the point (j, k) refers to the point $\sigma = (j/50)\, e^{i2\pi k/64}$; $0 \leqslant j \leqslant 50$, $0 \leqslant k \leqslant 64$. Thus the point $(0, k)$ $\forall k \in [1, 64]$ is the origin and $(51, k)$ $\forall k \in [1, 64]$ is the unit circle in the σ-plane.

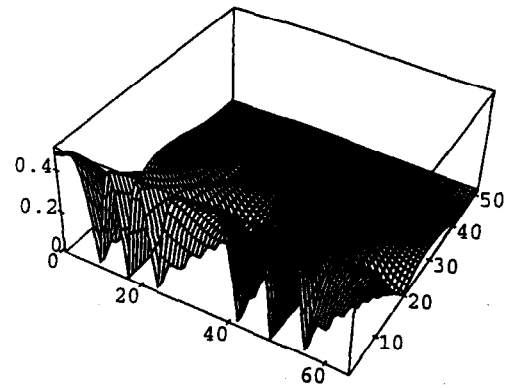

FIG. 2. Absolute value of the complex dilatation, $\lambda = 0.5\sigma^2 \sin(5(\sigma + \bar\sigma))$, where $\sigma = re^{i\alpha}$; $0 \leqslant r \leqslant 1$, $0 \leqslant \alpha \leqslant 2\pi$. The plot is shown here in rectangular co-ordinate system, where the point (j, k) refers to the point $\sigma = (j/50)\, e^{i2\pi/64}$; $0 \leqslant j \leqslant 50$, $0 \leqslant k \leqslant 64$. Thus the point $(0, k)$ $\forall k \in [1, 64]$ is the origin and $(51, k)$ $\forall k \in [1, 64]$ is the unit circle in the σ plane.

Therefore it follows that

$$h(\sigma) = \lambda(\sigma)(\ln z)_\sigma, \quad \sim O(\sigma^2) \qquad \text{as} \quad \sigma \to 0, \text{ if } \lambda(\sigma) \sim O(\sigma^3) \tag{48}$$

in support of our assumption that $h(\sigma)$ is in C_0^2.

3.3. Numerical Experiments

In this section we present some results of our numerical experiments on conformal and quasiconformal mappings with the numerical method of the previous section. In particular we have used Algorithm I discussed in the previous section. The results with Algorithm II, which is under implementation, are expected to be about the same. The numerical results to be presented for quasiconformal mappings will pertain to the following complex dilations:

$$\lambda_1 = |\sigma|^2\, e^{0.65(i\sigma^5 - 2.0)}, \tag{49}$$

and

$$\lambda_2 = 0.5\,|\sigma|^2 \sin(2.5(\sigma + \bar\sigma)). \tag{50}$$

TABLE I

Ellipse with Minor-Axis to Major-Axis Ratio: 0.6:1; $\lambda = \lambda_1$, tol = 1.0e–05

N	CPU time	Iterations	L^∞-error	L^2-error
16	1.2	13	0.427E−03	0.167E−03
32	3.0	14	0.802E−04	0.328E−04
64	8.6	16	0.183E−04	0.807E−04
128	22.0	15	0.463E−05	0.19E−05
256	71.7	16	0.114E−05	0.34E−06
512	239.7	16	—	—

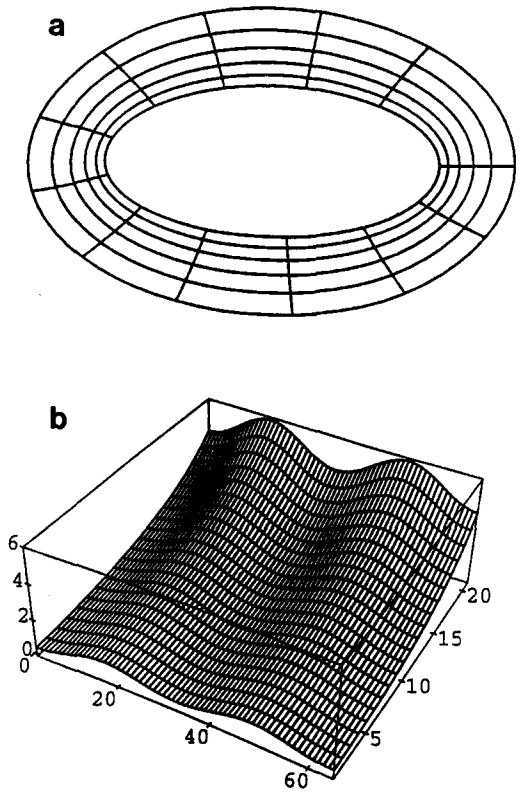

FIG. 3. Conformal mapping and associated Jacobian around the ellipse with minor axis to major axis ratio: 0.6:1. Some of the grids generated by conformal mapping of the interior of the unit disk onto the exterior of the ellipse are shown.

These functions are shown in Fig. 1 and Fig. 2, respectively, in rectangular co-ordinate systems, where (j, k) refers to $\sigma = (j/50)\, e^{2\pi ik/64}$. Note that both these functions decay rapidly away from the circle. The complex dilatation λ_1 behaves as required by our analysis of the previous section. Even though the complex dilatation λ_2 is $O(\sigma^2)$ as $\sigma \to 0$, numerically it is set to zero near the origin if its absolute value is less than 0.001. We should mention that we have done calculations with many dilatations and not all dilatations work on all profiles. However, quasiconformal mappings seem to succeed on many profiles with the above dilatations.

Even though we have done calculations over many profiles, we present results only for the following profiles exterior of which have been mapped conformally and quasiconformally onto the interior of a unit circle:

(1) An ellipse with minor-axis to major-axis ratio: 0.6:1

(2) Perturbed circle: $r(\alpha) = (1 + 0.08 \sin 4\alpha)\, e^{i\alpha}$; $0 \leqslant \alpha \leqslant 2\pi$.

Calculations have been carried out with $N = 16$, 32, 64, ..., 512 for each of $M = 11$, 21, 31, 41, 51. The results for these cases with $M = 51$ are presented in Tables I through IV. CPU times in the tables are in seconds on the MIPS computer which is approximately 15 times slower that the CRAY-YMP at Texas A & M University. Columns three and four in the tables give L^2 and L^∞ errors. The L^2 and L^∞ errors in these tables are measured with respect to the results obtained with $N = 512$.

The mappings for the case $N = 64$, $M = 51$ are presented in Fig. 3 through 8. In each of these figures, we have shown the images of some of the circular grids under the appropriate mapping mentioned in the figures. We have also shown the associated Jacobian of the mapping as defined by Eq. (42). The front view gives the Jacobian of the mapping on the innermost contour (i.e., the body). There are 65 grid points on each closed grid line.

TABLE III

Perturbed Circle: $r(\alpha) = (1 + 0.08 \sin 4\alpha)\, e^{i\alpha}$; $0 \leqslant \alpha \leqslant 2\pi$, $\lambda = \lambda_1$, tol = 1.0e–05

N	CPU time	Iterations	L^∞-error	L^2-error
16	1.5	15	0.527E – 03	0.237E – 03
32	3.1	14	0.102E – 03	0.499E – 04
64	7.6	14	0.238E – 04	0.106E – 04
128	20.7	14	0.609E – 05	0.276E – 05
256	63.3	14	0.127E – 05	0.563E – 06
512	212.8	14	—	—

TABLE II

Ellipse with Minor-Axis to Major-Axis Ratio: 0.6:1; $\lambda = \lambda_2$, tol = 1.0e–05

N	CPU time	Iterations	L^∞-error	L^2-error
16	1.3	13	0.315E – 03	0.183E – 03
32	3.3	15	0.562E – 04	0.302E – 04
64	8.41	16	0.157E – 04	0.892E – 05
128	23.3	16	0.462E – 05	0.218E – 05
256	71.6	16	0.103E – 05	0.452E – 06
512	239.1	16	—	—

TABLE IV

Perturbed Circle: $r(\alpha) = (1 + 0.08 \sin 4\alpha)\, e^{i\alpha}$; $0 \leqslant \alpha \leqslant 2\pi$, $\lambda = \lambda_2$, tol = 1.0e–05

N	CPU time	Iterations	L^∞-error	L^2-error
16	1.9	22	0.637E – 03	0.303E – 03
32	4.4	21	0.191E – 03	0.634E – 04
64	10.91	21	0.418E – 04	0.215E – 04
128	30.0	21	0.980E – 05	0.48E – 05
256	92.4	21	0.278E – 05	0.124E – 05
512	310.8	21	—	—

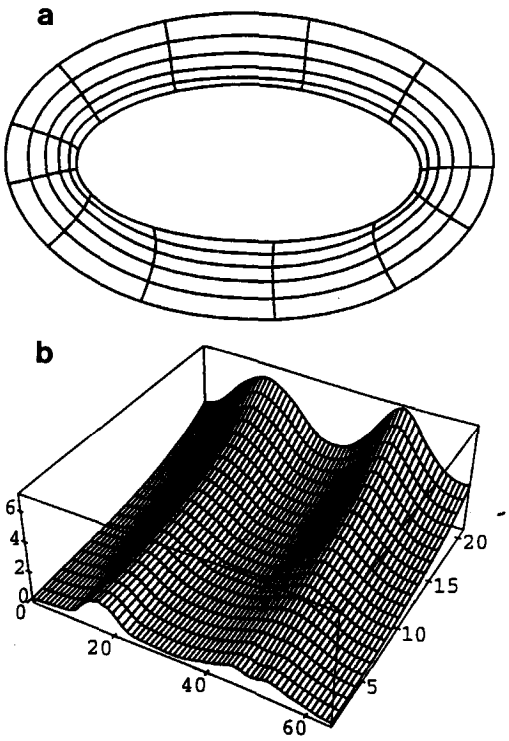

FIG. 4. Quasiconformal mapping and associated Jacobian around the ellipse with the dilatation shown in Fig. 1. Some of the grids generated by quasiconformal mapping of the interior of the unit disk onto the exterior of the ellipse are shown.

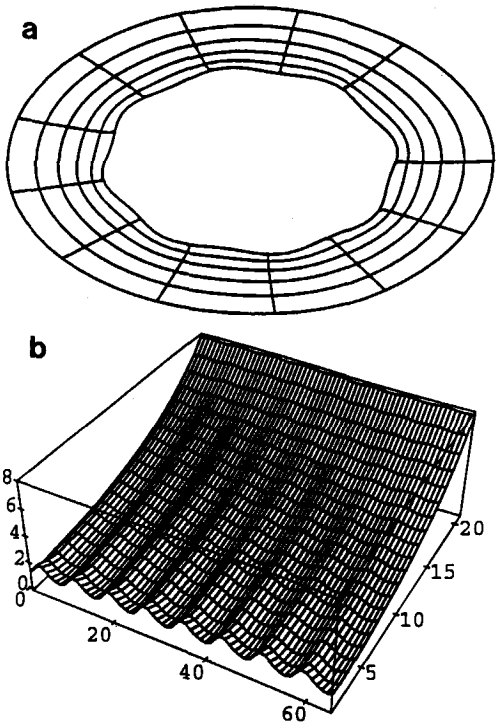

FIG. 6. Conformal mapping and associated Jacobian around the perturbed circle. Some of the grids generated by conformal mapping of the interior of the unit disk onto the exterior of the perturbed circle are shown.

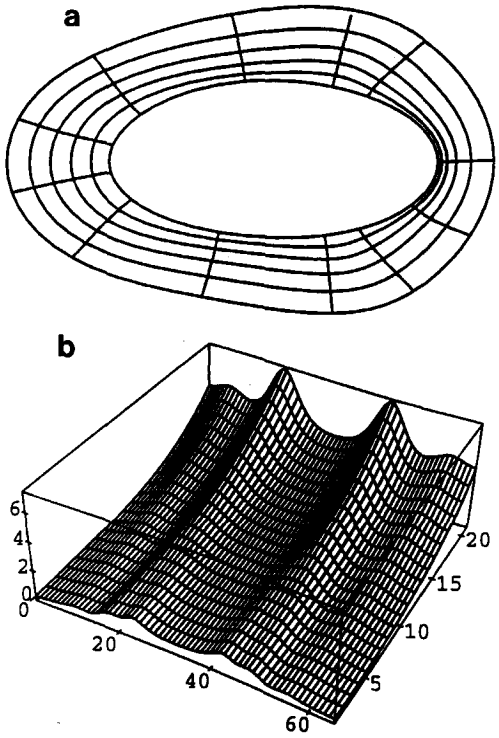

FIG. 5. Quasiconformal mapping and associated Jacobian around the ellipse with the dilatation shown in Fig. 2. Some of the grids generated by quasiconformal mappings of the interior of the unit disk onto the exterior of the ellipse are shown.

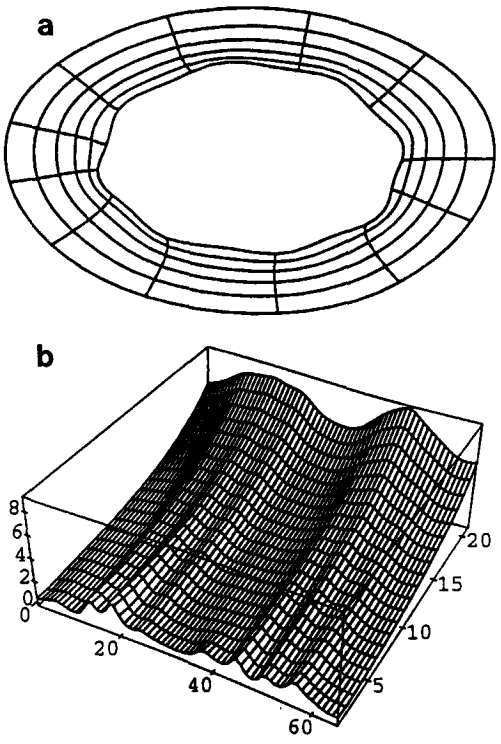

FIG. 7. Quasiconformal mapping and associated Jacobian around the perturbed circle with the dilatation shown in Fig. 1. Some of the grids generated by quasiconformal mapping of the interior of the unit disk onto the exterior of the perturbed circle are shown.

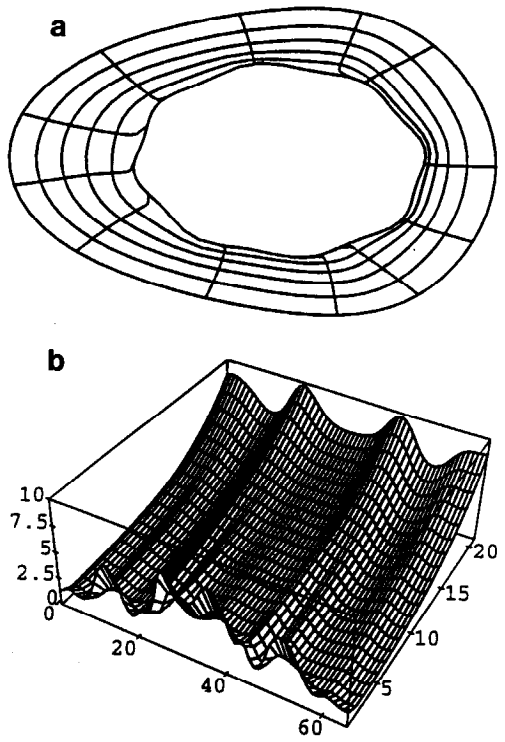

FIG. 8. Quasiconformal mapping and associated Jacobian around the perturbed circle with the dilatation shown in Fig. 2. Some of the grids generated by quasiconformal mapping of the interior of the unit disk onto the exterior of the perturbed circle are shown.

In Figs. 9 and 10, we show the Jacobian of the mappings on the surface of the profiles. We notice quite a few things in these figures and also in Figs. 3 through 8. The Jacobian of the mapping is symmetrical about the centerline for conformal mapping and the case of quasiconformal mapping with $\lambda = \lambda_2$. This is consistent with the theory since the dilatation and the profiles are symmetrical about the centerline. However, in the case of the Q-mapping with $\lambda = \lambda_1$, the Jacobian is not symmetrical because the dilatation λ_1 does not have this symmetry. In particular, we note that the absolute value of λ_1 is symmetric about the centerline, as shown in Fig. 1. In Figs. 9 and 10, we also show the surface values of the Jacobian for conformal maps. We see that for

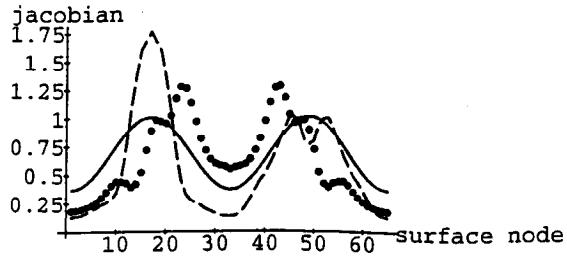

FIG. 9. The Jacobian of the conformal and quasiconformal mappings as a function of the nodes on the surface of the ellipse. There are 65 nodes on the surface. Sold line: conformal, dashed line: Q-map with $\lambda = \lambda_1$, dotted line: Q-map with $\lambda = \lambda_2$.

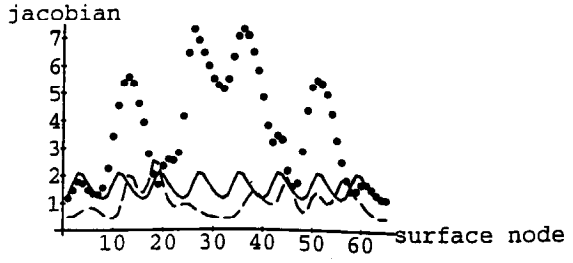

FIG. 10. The Jacobian of the conformal and quasiconformal mappings as a function of the nodes on the surface of the perturbed circle. There are 65 nodes on the surface. Sold line: conformal, dashed line: Q-map with $\lambda = \lambda_1$, dotted line: Q-map with $\lambda = \lambda_2$.

a Q-map with $\lambda = \lambda_1$, these values decrease almost everywhere for the case of a perturbed circle. However for the case of an ellipse, these values decrease over only a small portion of the ellipse. In fact, over some portion of the ellipse, the values of the Jacobian increase considerably. However, the effect of the Q-map with $\lambda = \lambda_2$ is quite different on these two profiles. Its effect on the surface values of Jacobian is stronger in the case of the perturbed circle than in the case of the ellipse.

In Figs. 11 and 12, we show the convergence rates of the algorithm for these quasiconformal mappings. In case of the ellipse, the mappings with these dilatations have significantly different rates of convergence initially. However, in the case of the perturbed circle, the dilatations seem to have no effect on the rates of convergence.

We make the following observations from these figures and tables:

(1) The number of iterations seems almost independent of the number "N" of nodes on the body, with the complex dilatation fixed.

(2) The number of iterations may depend strongly or weakly on the complex dilatation according to the shape of the body.

(3) The CPU time seems to be of the order of our theoretical estimate $O(N \ln N)$ for small N and slightly higher than this estimate for large N. Slightly higher estimate for large N is due to excessive amount of high data-output associated with these cases.

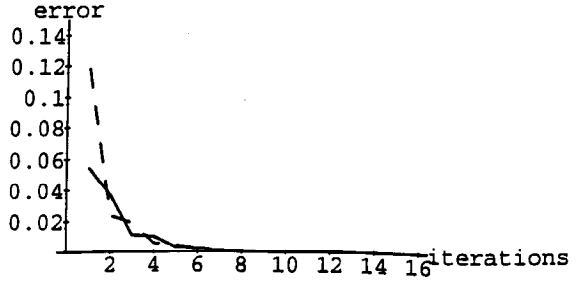

FIG. 11. L_∞ error as a function of the number of iterations for quasiconformal mappings of the ellipse. Dashed line with $\lambda = \lambda_1$, solid line with $\lambda = \lambda_2$.

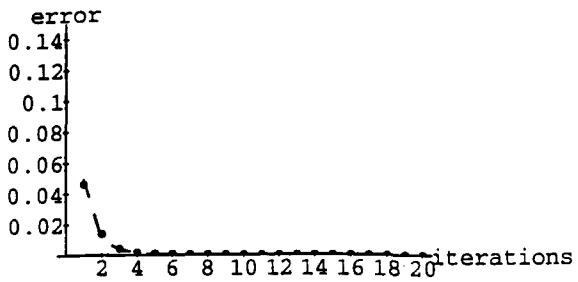

FIG. 12. L_∞ error as a function of the number of iterations for quasiconformal mappings of the perturbed circle. Dashed line with $\lambda = \lambda_1$, dots with $\lambda = \lambda_2$.

(4) The Jacobian of the mapping can be adjusted easily by changing the value of the complex dilatation. This extra flexibility will allow one to control the crowding phenomenon associated with the Jacobian of the mapping.

(5) The same dilatation may have different effects on different profiles.

4. CONCLUSIONS

In this paper we have presented two fast algorithms to solve the boundary value problems associated with the Beltrami equation (1). We have also provided a fast algorithm to evaluate the principal value integral that arises in these problems. We have shown that this problem is the building block for constructing quasiconformal mappings, and we have presented a method for such mappings. Numerically we have constructed quasiconformal mappings for various profiles and various dilatations. Some results have been presented. In particular we have shown the effect of dilatations on the Jacobian of the mappings which controls what is known as the crowding phenomenon in the literature. Currently we are undertaking generalizations of various conformal mapping methods to the quasiconformal case and a detailed numerical study of these will be reported in the future.

ACKNOWLEDGMENTS

This research has been supported in part by NSF Grant DMS-9107819. It is a pleasure to thank Natarajan Sivakumar for proofreading the manuscript.

REFERENCES

1. L. V. Ahlfors, *Lectures in Quasiconformal Mappings* (Van Nostrand, New York, 1966).
2. P. P. Belinskii, S. K. Godunov, and I. K. Yanenko, *USSR Comput. Math. Phys.* **15**, 133 (1975).
3. L. Bers, *Mathematical Aspects of Subsonic and Transonic Gas Dynamics*, 1958.
4. R. Courant and D. Hilbert, *Methods of Mathematical Physics, Vol. II* (Wiley, New York, 1961).
5. P. Daripa, *J. Comput. Phys.* **88**, 337 (1990).
6. P. Daripa, *J. Comput. Phys.* **96** (1991), pp. 229–236.
7. P. Daripa, *SIAM J. Sci. Stat. Comput.*, Nov. (1992).
8. M. H. Gutknecht, *SIAM J. Sci. Stat. Comput.* **4**, 1 (1983).
9. P. Henrici, *Applied and Computational Complex Analysis, Vol. 3* (Wiley, New York, 1986).
10. S. Krushkal, *Quasiconformal Mappings and Riemann Surfaces* (Cambridge Univ. Press, New York, 1961).
11. J. Lawrynowicz, *Quasiconformal Mappings in the Plane*, Lecture Notes in Mathematics, Vol. 1039 (Springer-Verlag, New York/Berlin, 1983).
12. C. W. Mastin and J. F. Thompson, *Quasiconformal mappings and grid generation, SIAM J. Sci. Stat. Comput.* **5**, 305 (1984).
13. L. C. Woods, *The Theory of Subsonic Plane Flow* (Cambridge Univ. Press, New York, 1961).